

Integrating the artificial intelligence and hybrid machine learning algorithms for improving the accuracy of spatial prediction of landslide hazards in Kurseong Himalayan Region



Anik Saha, Sunil Saha *

Department of Geography, University of Gour Banga, Malda, India

ARTICLE INFO

Keywords:

Multilayer perception
Kernel logistic regression
Random forest
Multivariate adaptive regression splines
Hybrid algorithms

ABSTRACT

The aim of the current work is to compare susceptibility maps of landslides produced using machine learning techniques i.e. multilayer perception neural nets (MLP), kernel logistic regression (KLR), random forest (RF), and multivariate adaptive regression splines (MARS); novel ensemble approaches i.e. MLP-Bagging, KLR-Bagging, RF-Bagging and MARS-Bagging in the Kurseong-Himalayan region. For the ensemble models the RF, KLR, MLP and MARS were used as base classifiers, and Bagging was used as meta classifier. Another objective of the current work is to introduce and evaluate the effectiveness of the novel KLR-Bagging and MARS-Bagging ensembles in susceptibility to landslide. Compiling 303 landslide locations to calibrate and test the models, an inventory map was created. Eighteen LCFs were chosen using the Relief-F and multi-collinearity tests for mapping the landslide susceptibility. Applying receiver operating characteristic (ROC), precision, accuracy, incorrectly categorized proportion, mean-absolute-error (MAE), and root-mean-square-error (RMSE), the LSMs were subsequently verified. The different validation results showed RF-Bagging (AUC training 88.69% & testing 92.28%) with ensemble Meta classifier gives better performance than the MLP, KLR, RF, MARS, MLP-Bagging, KLR-Bagging, and MARS-Bagging based LSMs. RF model showed that the slope, altitude, rainfall, and geomorphology played the most vital role in landslide occurrence comparing the other LCFs. These results will help to reduce the losses caused by the landslides in the Kurseong and in other areas where geo-environmental and geological conditions more or less similar.

1. Introduction

Landslides are more destructive yet frequent natural hazards in the Himalayan region, causing remarkable harm to buildings, property, and the human lives (Chawla et al., 2018). In India, mountainous regions such as Jammu & Kashmir, Uttarakhand, Himachal Pradesh, the northern portion of West Bengal, Sikkim, and the northeastern states are heavily threatened by landslides. According to Froude's work (2018), 75% of global semi-seismic landslides from 2004 to 2016 were recorded in seven south-east developing countries (they are India, China, Laos, Bangladesh, Myanmar, Philippines, and Indonesia) (Chauhan et al., 2018; Aristizábal and Sánchez, 2020). It is believed that around 500 lives and around Rs.300 Crores (approx. US\$ 3 billion) worth of properties have been damaged annually due to landslides (Koley et al., 2019; Khamkar and Mhaske, 2019). India's most landslide prone areas has found in Himalayan mountain region (Saha and Saha, 2020a).

There is a huge number of techniques and simulations applied for formulating the reduction or mitigation plans for landslide damage (Khamkar and Mhaske, 2019; Liao and Liao, 2020; Saha et al., 2020). Managing the landslide hazard zones (LHZs) needs concerted efforts, while, landslide susceptibility mapping (LSM) is a prevailing tool and most useful technique for reducing the effects of landslides (Pecoraro et al., 2019). Those mappings assist in the visualization and regional prediction of landslide hazards in a particular province (Chawla et al., 2018). LSM is predicated on the presumption that future landslides would occur under similar conditions to those that produced prior landslides (Pham et al., 2016; Hirota et al., 2019). Only the LSM shows the geographical position of landslide threats in a particular mountainous area that are generated by their local climate and influencing factors (Pham et al., 2016). A number of parameters including location, climatic conditions, landslide types and geo-environment need to be evaluated for monitoring of landslide sensitivity region (Mahdadi et al., 2018).

* Corresponding author.

E-mail addresses: aniksahamalda@gmail.com (A. Saha), sunilgeo.88@gmail.com (S. Saha).

Primarily the configuration of underlying geology (lithological composition, formation, extent of weathering), geomorphology (slope orientation, relative relief, and appearance), soil type (deepness, composition, porosity, and permeability), LULC and climatologically properties are important intrinsic factors for landslides (Reichenbach et al., 2018; Amato et al., 2019; Ozioko and Igwe, 2020; Saha et al., 2021). Preparation of LSM and selection of landslide conditioning factors using ML method can enhance the effectiveness of landslide risk reduction

engineering procedure. Wang et al. (2019) applied a insensitive set hypothesis to less significant landslide factors. Saha et al. (2022) utilized a chi-square-based factor selection technique to screen key factors.

Mapping and identifying the high-risk zone of landslide is a scientifically accepted practice that aim to provide the scientific basement for planning and enhancement of the area (Koley et al., 2019; Juliev et al., 2019). Modeling with the simulation of landslide susceptibility has effectively allowed in the last few years to reduce the damages (Juliev

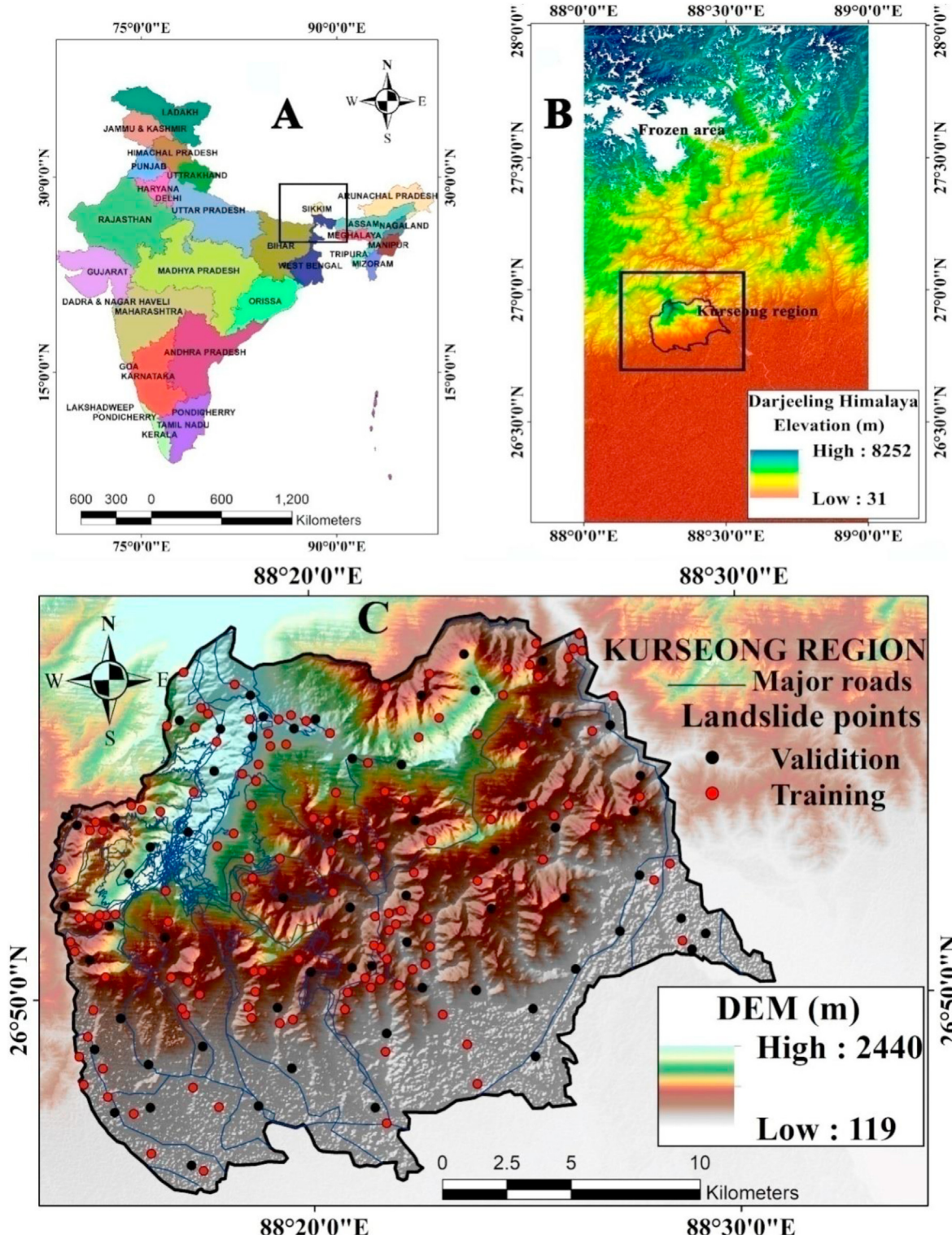


Fig. 1. Location of the study area (A) India; (B) Darjeeling Himalaya; and (C) Kurseong region with landslide inventory.

et al., 2019). Researchers have developed many statistical methods to solve landslide problem (Chawla et al., 2018). Semi-quantitative techniques are depended on weighting and rating of the factors for example Analytical hierarchy process, combined landslide Frequency ratio, Information value, Weight of evidence, Fuzzy logic approach and weighted linear combination process (Chen et al., 2016; Mahdadi et al., 2018; Saha and Saha, 2020a). In recent decades, researchers applied machine learning techniques (MLT) to identify the LHZs in landslide prone region in all over the world (Sevgenet et al., 2019; Saha et al., 2021) including Support vector machine (Meng et al., 2016; Saha and Saha, 2020c), Decision trees (Khosravi et al., 2018; KutlugSahin and Colkesen, 2019); Kernel logistic regression (Chen and Chen, 2021) Random forest (Kornejad et al., 2019; Saha et al., 2020), Multivariate adaptive regression splines (Liao and Liao, 2020) and Artificial neural network (Srivastava et al., 2019; Saha et al., 2020). The MLT have been given better accuracy than previous probabilistic models (Mahdadi et al., 2018; Saha et al., 2022). In the case of landslide study, different MLT play different accuracy in different place.

LSM is the main purpose of this research for Kurseong area of Darjeeling Himalaya, applying the MLP, KLR, RF, MARS, MLP-Bagging,

KRL-Bagging, RF-Bagging and MARS-Bagging models. Ensemble hybrid machine learning is rare, especially in the Indian Darjeeling Himalayan region, MLP-Bagging was used in land subsidence susceptibility in Iran (Arabameri et al., 2020); RF-Bagging was applied in flood susceptibility modeling in Bangladesh (Talukdar et al., 2020) and KLR-Bagging & MARS-Bagging are novel ensembles and still not used in landslide modelling. In this research an ensemble was made between bagging meta classifier and all the used models (MLP, KLR, RF and MARS) for modeling landslide susceptibility due to exceptional performance of ensembles of Meta classifier and AI model. For comparing and evaluating the outcomes of these models, receiver operating characteristics (ROCs), precision, accuracy, Kappa coefficient, RMSE, MAE techniques, and seed cell area index (SCAI) were employed. In the main purpose of the work was to show whether the accuracy level of benchmark models i.e. MLP, KLR, RF, and MARS increases or decrease after combining with the hybrid meta classifier (bagging). Additionally, there is an involvement in checking how these models in realistic conditions fluctuate in their predictive effectiveness. A significant deluge is observed in the Kurseong range of Darjeeling Himalayan during the period of the research, where hundreds of large and minor landslides were recorded. The landslides linked to the

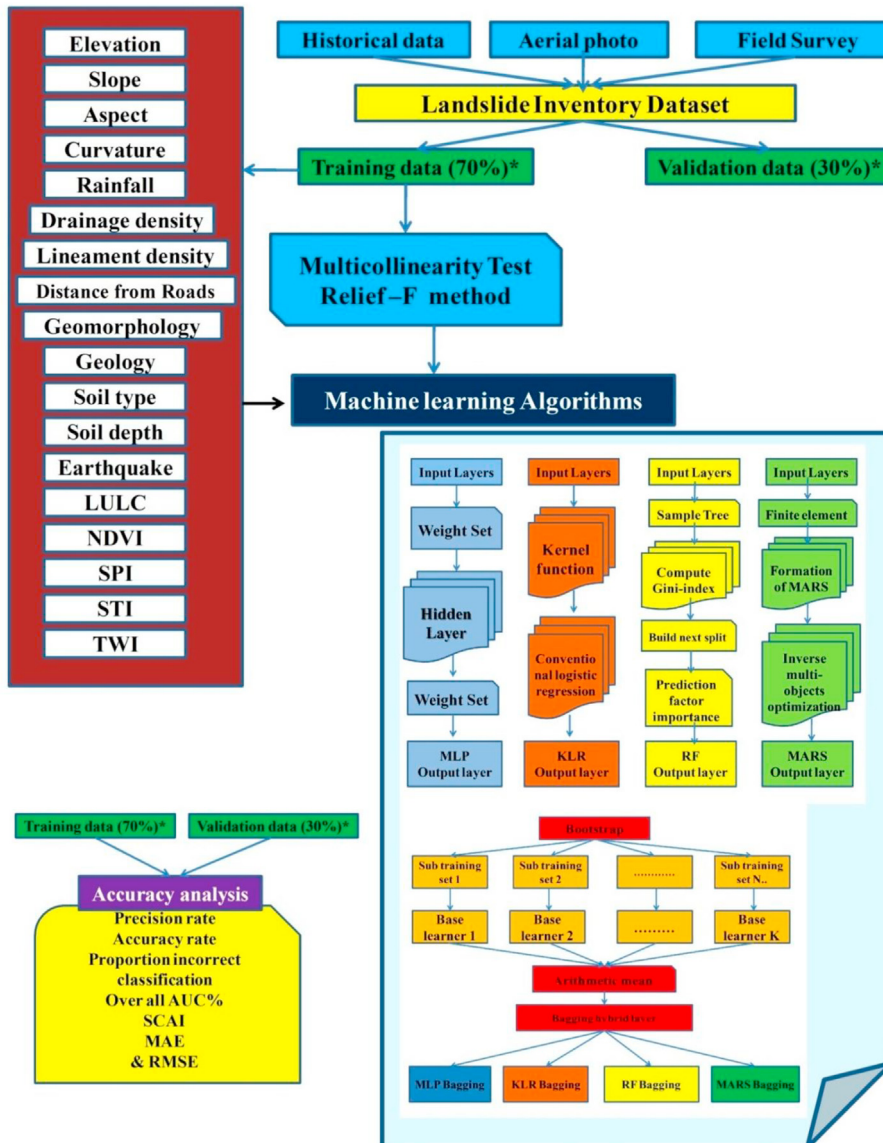


Fig. 2. Methodological flowchart of the study.

(MLP = Multilayer Perception; KLR = Kernel Logistic Regression; RF = Random Forest; MARS = Multivariate Adaptive Regression Splines; SCAI = Seed Cell Area Index; MAE = Mean Absolute Error; & RMSE = Root Mean Square Error).

2020 deluge have therefore been obtained and used to evaluate the accurateness of the used models.

2. Study area

Kurseong region (Fig. 1) is covered 380.34 km²area of Darjeeling-Himalaya of India (latitudes 26°46'30"N to 26°57'47"N and longitudes 88°08'25"E to 88°27'54"E). Kurseong Municipality is at an elevation of 1458 m and 31.54 km from Darjeeling, a sub-divisional town. The mean maximum temperature is 23.69 °C, mean moisture ranges from 68 to 92%, and 323.5 cm is the annual average precipitation (Municipal weather database from 1982 to 2017) of the study area. The climate in the region is associated with the CWA (Monsoon-influenced subtropical humid climate) group of Koppen. About 85% of the yearly precipitation takes place between 2nd of June to end of august. The slope is very steep (40° to 69°) and the mean slope for the whole area is 23.76°. The region is characterized by the sculptured degraded landscape in its young stage of morphology down-cutting by the stream flows and rivers

together with pre-existing deformities in a geological system including rocks of Darjeeling gneiss and Daling sequence of Archaean, Gondwana rocks of Permian, Siwalik rocks and Pleistocene elevated terrace (GSI, the year 2005-06). Nearly 93% of the total area (355.79 km²) is mountainous underneath the Himalayan and 50.43% is covered by intense forest and open forest. The landslide frequently affects the area of the study and does enormous damage to infrastructure and agriculture (Fig. 2). This area needs immediate deployment of landslide mitigation planning. For such management strategies, landslide susceptibility mapping is important for identifying the area most prone to landslides.

3. Materials and methods

The study's methodology comprises main six phases: (1) Preliminarily, the previous pieces of literature were studied to select some landslide conditioning parameters and collect various data from a different source; (2) The data were obtained through a series of field investigation with the help of handheld GPS after the collection of landslide condition



Fig. 3. Landslide field photos (2019-20) of study area(A) Rohini road (26° 52'23"N; 88° 21' 01"E); (B) Municipality road (26° 52'28"N; 88° 22' 29"E) (C) Near NH 55 (26° 42' 27"N; 88°23'19"E), (D)Kurseong to Darjeeling municipality road (26°52'32"N, 88°20'17"E).

factors (LCFs); (3)Afterward, these LCFs were tested by the multi-collinearity analysis and relief-F. In the third step, the thematic layers of LCFs were prepared; (4) The benchmark models i.e. MLP, KLR, RF, and MARS simulations were used for the modeling of landslide susceptibility; (5) hybrid MLT (Bagging) was an ensemble with MLP, KLR, RF and MARS (Fig. 2); (6) In the next step the produced models were tested applying AUC-ROC values, MAE, RMSE, proportion incorrectly classified, precision and accuracy validation methods. After validation, the LSMs were judged with the deluge of September 2020.

3.1. Landslide inventory map of Kurseong

For any type of landslide modeling, the relationship between LCFs and the distribution of earlier landslides must be assessed (Chen et al., 2016; Saha et al., 2022). So the inventory map with 303 previous landslides was used in this study. Via field surveys with a global positioning system (GPS) from April 2016 to February, 2020, such landslide locations were verified (Fig. 3). In addition, previous information on landslides and disaster reports from the National Disaster Management Authority (NDMA) and the Darjeeling District Offices were gathered. The inventory map and LCFs were created at a standard scale of 30 m *30 m. After collecting the landslide data 70% of landslides (212 points) were used to run the models and 30% were used for testing the methods (equivalent to 91 landslide points). The Geo-statistical analysis feature of ArcGIS version 10.3 was used to figure out the training and testing sites (Fig. 1C).

3.2. Factors selection for LSMs modeling

The choice of LCFs among the various factors used by the different researchers is a challenging process since there are no standardized criteria. Tien Bui et al. (2019) and Saha and Saha (2020a) used mathematical methods to choose the important LCFs. In all areas, the same environmental, geological and hydrological variables are not applicable and cannot be used for mapping all hazards (Arabameri et al., 2020). To recognize certain geo-environmental factors, Saha et al. (2020) used the Relief F-test. Different analysis techniques can be used for evaluating parameters such as correlations, relief-f, IGF, probabilistic techniques, and machine learning algorithms. The multi-collinearity (MC) test and relief-F are being used to identify the LCFs.

3.2.1. Testing multi-collinearity (MC) problem

The MC technique is a procedure for assessing the variables. Due to higher associations between LCFs, the estimation of land susceptibility area may be inaccurate (Dang et al., 2020; Saha and Saha, 2020c). MC decides the independence of the LCFs. Pearson coefficients of correlation, percentages of variances, variance inflation factors (VIF) with conditional index, and tolerance levels can be utilized to measure the MC (Cama et al., 2016; Sameen et al., 2020). The VIF and tolerance processes were applied to estimate MC in this region. The VIF and TOL (tolerance) threshold values considered to measure the MC are $VIF \leq 5$ and tolerance ≥ 0.2 (Bui et al., 2016; Saha et al., 2022).

3.2.2. Relief-F method

The Relief-F technique was used as another factor-selection method. This method synthesizes weights according to factor ability. Assume that 'S' is a randomly chosen sample. Next, the Relief-F weight RW_i for the i -th feature is measured by equation (1). One random point could determine the two closest neighboring points (one of them being of the same class; another of various classes).

$$RW_i \leftarrow Wi + |S^i - NM^i| - |S^i - NM^j| \quad (1)$$

where NH is the nearest hit and NM is the nearest miss

Kononenko (1994) proposed several Relief-F models. Experimental findings have also shown that Relief-F works equivalent to the initial Relief (Wang et al., 2016).

3.3. Landslide conditioning factors (LCFs)

The different type of landslide (LS) happens due to an imbalance in the local factor's resistance and mechanisms (Pisano et al., 2017). In this research, some specified geo-environmental LCFs were selected for recognizing LS hazard zone and mapping. The most important selected factors for this study are presented below.

SRTM DEM of 30*30 m resolution was used for evaluating the LS susceptibility. It was collected from the USGS (www.usgs.org). Four LCFs (Fig. 4A; 4 B; 4C; and 4D) were obtained from the DEM, including altitude, slope, aspect, and curvature.

For the annual precipitation map (Fig. 4E) 35 years (1982–2017) of monthly average rainfall data were arranged from the Indian Metrological Department (https://mausam.imd.gov.in/imd_latest). Generally, in landslide vulnerability analysis, rainfall in the mountainous areas is regarded as a significant triggering factor for landslide hazards (Lin et al., 2012). The drainage structures are a natural consequence of the long-standing slope, geographical features, landscape, and landform interactions. Drainage density was measured by calculating the whole length of the drainage by the study's total area (Fig. 4F). Similarly, the lineament density was calculated and classified into 5 divisions (Fig. 4 G).

The highways, developed on a very steep slope, undermine the land protection above them. The risk of topographical loss increases as the slope of the region increases. This research divides the distance from the roads into five groups (Fig. 5H). The soil properties are a very powerful conditioning element for measuring the vulnerability of landslides (Ozioko and Igwe, 2020). In this area of study, four forms of soil, i.e. WO02 (Loamy skeletal, Typic Udoorthents, Loamy skeletal, Typic Dystrochrepts), WO04 (Loamy-skeletal, Typic Udoorthents, Loamy skeletal, Typic Haplumbrepts) and WO06 (Course loamy, Umbria Dystrochrepts) were founded, depending on the taxonomy. Two factors related to soil namely, soil types (Fig. 4I) (Table 5) and soil depth (Fig 4L) were prepared. Soil category datasets were obtained from the NBSS & LUP. A field study was done to produce the soil depth map (Fig 4L). The present geological map (1: 50,000) was resampled to the resolution of 30 m. From the Survey of India research area's geological map was obtained. Gneiss, Slate & Schist, Damuda, Limestone, and Alluvial are the geological segments found in this study area (Fig. 4I). The research region's geomorphological map (Fig. 4J) is extracted from Bhuvan (<http://bhuvan.nrsc.gov.in>) produced by ISRO (Indian Space Research Organization) and the Ministry of Mines together with 15 collaborator institutions. The study field is divided into various moderate and narrow spurs; ridges, deep valleys formed by 'V', and other degradation features. LS frequency also revealed a connection with seismic activity, fault dip-flow, and mountain slope orientation. The Medvedev–Sponheuer–Karnik method is the macro-seismic strength measure, popularly known as the MSK scale. It is implemented for an assessment of the severity of the Earthquake, focusing on the impact of the incident on the province. In 2011 to 2018 five earthquake happened in this region and it triggered 13 landslides and among them Tista lineament seismic wave caused more damage (Table 1). Using the supervised classification method the LULC map was prepared. Eight classes of the LULC were found. These classes are settlement (7.82%), plantation farming (17.13%), open forest (26.84%), agricultural land (12.83%), fellow land (4.10%), sandbar (2.86%) and water body (4.02%), respectively.

The stream power index (SPI) (Fig. 4N), sediment transport index (STI) (Fig. 4O), and the topographic wetness index (TWI) (Fig. 4P) were regarded as significant conditioning factors for the preparation of LSMs (Nsengiyumva et al., 2019). These maps were built from the DEM in ArcGIS.

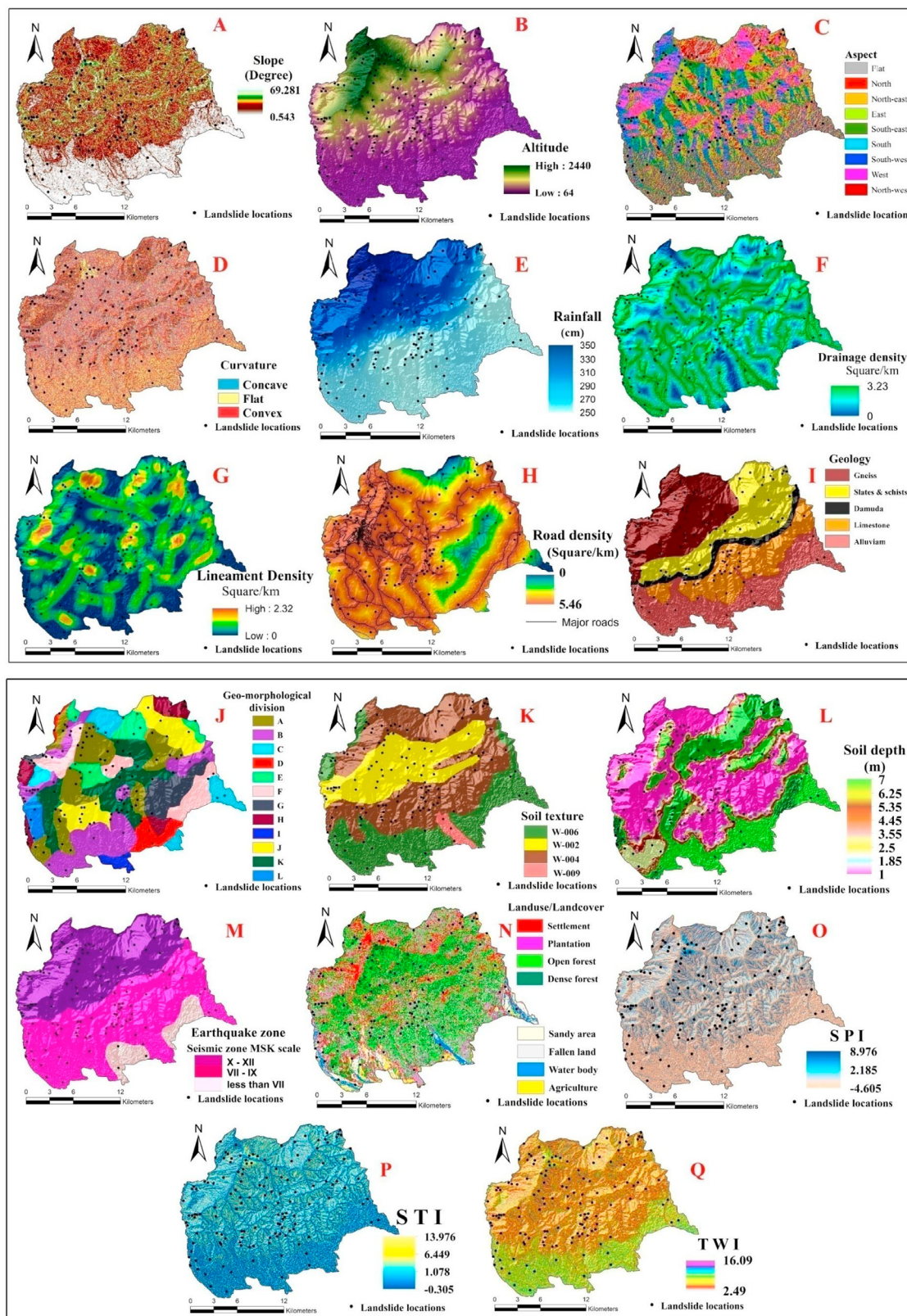


Fig. 4. Landslide conditioning factors: A. Slope, B. Elevation, C. Aspect, D. Curvature, E. Rainfall, F. Drainage density, G. Lineament density, H. Distance from road, I. Geology, J. Geomorphology (A = Deeply entrance denudation valley; B = Moderately dissected valley; C = Fault related faceted slope; D = Alluvial deposition fan; E = Dissected screenland slope; F = Lowly inter mountain valley; G = Old alluvial deposition terrace; H = Alluvial debris intermountain fan; I = Deposition alluvial flood plain; J = Fluvial denudation mountain valley; K = Intermountain moderate slope structural plateau; & L = Alluvial debris deposition new plain), K. Soil type, L. Soil depth, M. Earthquake zone, N. Land use/Land cover, O. SPI, P. STI and Q. TWI.

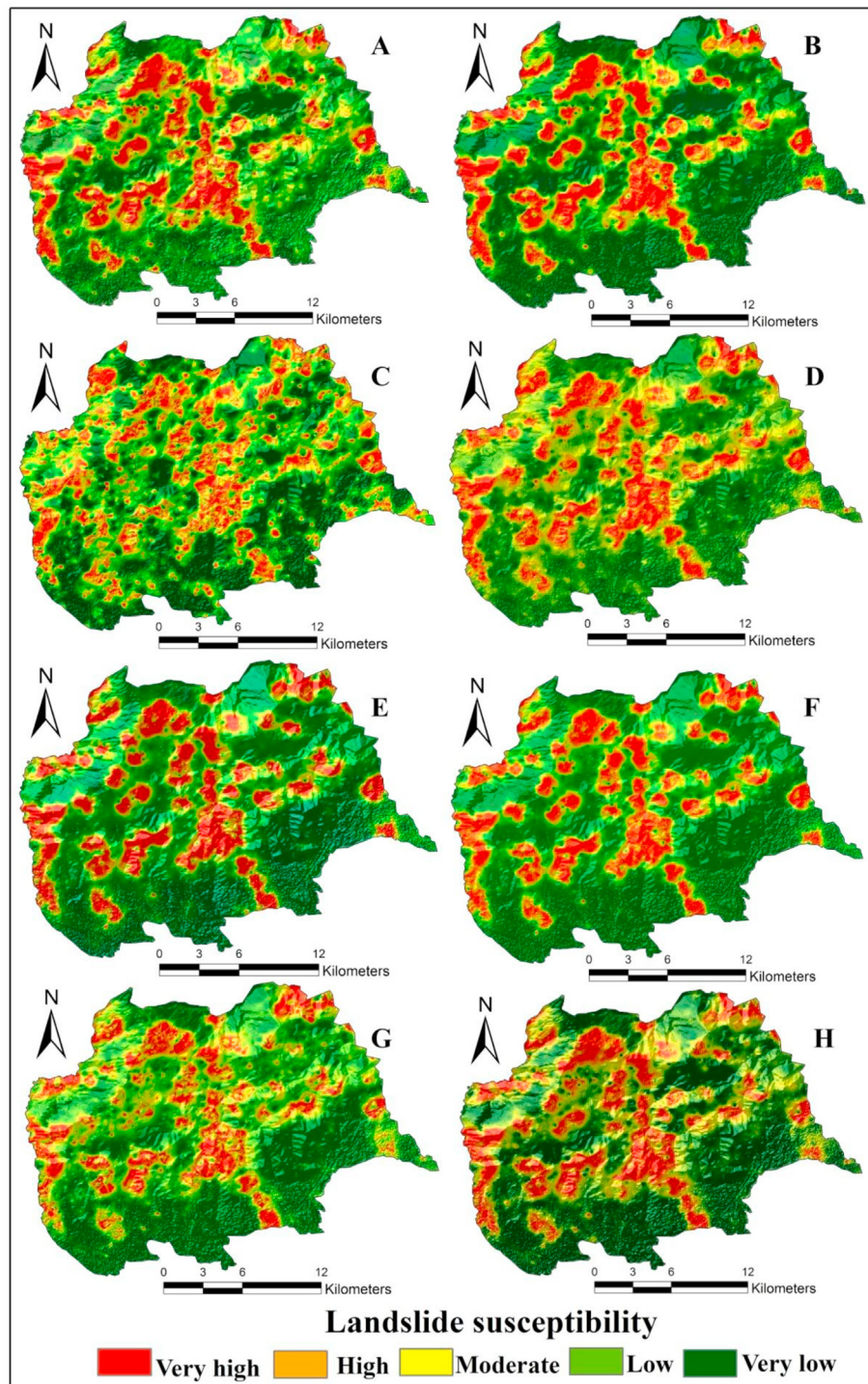


Fig. 5. Landslide susceptibility mapping produced by A. MLP model; B. MLP-Bagging model, C. KLR; D. KLR-Bagging model; E. RF model; F. RF-Bagging model; G. MARS model; and H. MARS-Bagging.

3.4. Machine learning methods

3.4.1. Multilayer perception (MLP)

Users, commonly used for grouping, are familiar with multi-layer perception (MLP) as ANNs (Haykin, 2009). The training sets are not dependent on the hypothesis of the statistic distribution of the input variables, the relative significance of those input variables is not defined, and the factors are chosen based on their weights throughout the test procedure (Gardner and Dorling, 1998). Input, hidden, and output layers constitute and construct the MLP. The geo-environmental LCFs are the

input layers and LS or non-LS are the output layers. The hidden layers are classified and helped to transfer data into output. MLP development is divided into two stages (Tien Bui et al., 2019; Zhou et al., 2018; Pham et al., 2016): 1) The performance values are transmitted from the hidden layers and the result values are then incorporated with the preceding values for the differentiation and 2) the correlation weight is associated to produce the best results at the lowest distance. where $X = X_i$, $i = 1.....18$ is the vector of the 18 LCFs, $y = 1$ or 0 , indicating LS or non-LS. Applying equation (2) the MLP was carried out.

Table 1

Details of Earthquakes accelerated landslide in Kurseong region.

Earthquake date	Seismic sources	Magnitude (Epicenter)	No. of Landslide	Total damage
18/09/2011	Tista Lineament	6.9 Mw	6	Comparatively high damage
06/02/2017	Main Boundary Thrust (MBT)	5.1 Mw	3	Moderate damage
03/01/2017	Main Central Thrust (MCT)	5.7 Mw	2	Minor damage
12/05/2015	Purnaea Everest Lineament (PEL)	7.7 Mw	1	Building damaged
12/09/2018	Saptegram, Assam	5.3 Mw	1	Minor damage

Source: National Center of Seismology, Ministry of Earth Science, Govt. of India; Newspaper- Hindustantimes & Indiatoday

$$y = f(X) \quad (2)$$

where, $F(X)$ is assumed to be a hidden mechanism that progresses by modifiable weights during the network architecture training process. In our study, to prevent overfitting, 1 hidden layer, 500 epochs, and 20 validation thresholds obtained by trial-and-error were fitted with an MLP.

3.4.2. Kernel logistic regression (KLR)

KLR is an efficient and scalable discriminative approach that can have good class prediction (Sugiyama and Simm, 2010). Mercer kernel suggested a traditional logistic regression model built-in high-dimensional feature space (Mercer, 1909). Given the labeled training information, need to do the following:

$$D = \{(x_i, y_i)\}, i = 1, x_i \in X \in R^d, y_i \in [0, 1] \quad (3)$$

where, the landslide conditioning factor is represented by x_i and in the function space, $K : X \times X \rightarrow R$ computes the kernel function of the values of the input vectors.

The isotropic radial basis function (RBF) was utilized as the kernel function in this study:

$$K(x, x') = e^{-\xi \|x - x'\|^2} \quad (4)$$

Then, in the feature space, a standard logistic regression model was built as follows:

$$\text{logit } \{h(x)\} = \omega \cdot \varphi(x) + c, \text{ logit } (p) = \log \frac{p}{1-p} \quad (5)$$

where optimal model parameters are represented by (ω, c) .

3.4.3. Random forest (RF)

The RF is an essential machine learning process that produces accurate predictions without the curse of dimensionality (Shahbazi et al., 2017). RF model works on the concept of classification trees. RF reliably compares, tests, and deals with inconsistency and imprecision in diverse data sets (Lin et al., 2015). RF models create a range of decision trees with a mean decrease in the Gini index (Cutler et al., 2007). At each branching node, RF models take into consideration a random subset of the input data and allow the tree to grow without limiting the tree's maximum size (Rodriguez-Galiano et al., 2012). RF begins with the bagging process in which sub-samples of bootstrap are randomly chosen to be checked and the unused sub-samples for assessment of 'Out of Bag' or OOB are taken into consideration. The utility of each OOB error adjustment pattern is measured first. Stability is considered to be confirmed by the randomized bagging process (Breiman, 1996). BT A log (N), which includes the number of training samples (training group LS occurrences), trees, and nodes, respectively, in each division represented

by B, T, and A (Chan and Paelinckx, 2008). Chen et al. (2016) identified the advantages of using 'OOB' error and assessment process: no overfitting errors, low bias and variance, a limited association between individual trees, rigorous estimates of error, and excellent prediction performance. Afanador et al. (2016) also prepared functional algorithms for the RF model. In this analysis, RF modeling was conducted using the 'random Forest' package of R studio (Genuer et al., 2010).

$$BT \propto A \log(N) \quad (6)$$

3.4.4. Multivariate adaptive regression splines (MARS)

Friedman and Roosen (1995) were the first to introduce MARS. In a similar way to least-squares regression, It investigates the connection between both the variables of the study (Wang et al., 2021). MARS' benefits include its numerical effectiveness, ability to produce simple-to-understand models, and ability to measure the contribution of predictor variables. However, one of the most notable disadvantages is its inability to forecast accurately (Nguyen et al., 2021; Wang et al., 2021). To fix this issue, bagging was applied to MARS, resulting in MARS-Bag, which increased classification accuracy.

3.4.5. Ensemble of MLP, KLR, RF, and MARS with Bagging

Bagging, introduced by Breiman (1996), was assigned to forecast LS sensitivity, one of the appropriate and efficient-ensemble techniques. To direct individual classifiers, the Bagging process utilizes bootstrap samples. New subsets of MLP, KLR, RF, and MARS training data were collected by randomly sampling the training sets with replacements. As the training base-classifier, certain sub-training sets were included. To incorporate the result of the base classifier, plurality voting was used (Breiman 1996). As the base classifier of the Bagging ensemble meta classifier, MLP, KLR, RF, and MARS MLT was used to compare the results with the individual MLP and RF models.

3.5. Validation computed process

Validation is important if model reliability is to be calculated (Groesser and Schwaninger, 2012; Saha et al., 2020). Two statistical approaches (MAE and RMSE) and three threshold-dependent statistics (area under of ROC curve, proportion incorrectly classified, accuracy, and precision) were used to determine the reliability of the models in this analysis.

3.5.1. Threshold dependent method ROC

The techniques used to assess the zones of susceptibility need to be checked (Meng et al., 2016). Here more than one validation process was applied for judging the prediction capability and it is more acceptable to all for supporting the models. The pieces of literature ensured that the AUC of ROC is a useful method for model validation and comparison (Marjanović, 2013; Gayen et al., 2019). The AUC was calculated applying equation (7).

$$AUC = \frac{(\sum a + \sum c)}{(P + N)} \quad (7)$$

where a is 'a true positive', b is 'a true negative', c is 'a false positive' and d is 'a false negative'. P is 'the amount of LSs overall', and N represents 'the number of non-LSS overall'.

$$Precision = \frac{a}{(a + b)} \quad (8)$$

$$Accuracy = \frac{(a + c)}{(a + b + c + d)} \quad (9)$$

The AUC values range from 0 to 1 and the value closest to 1.0 implies a model's higher efficiency. The reliability of forecasting analytics and their reliability were also tested using proportion incorrectly classified,

accuracy and precision. Higher values of both accuracy and precision suggest that the model has greater predictability. On the other side, lower values proportion incorrectly classified suggest greater precision.

3.5.2. Statistical techniques MAE & RMSE

MAE and RMSE in this analysis were used to test the models. Some of the discrepancies between predicted and actual values are called MAE. MAE's square root is expressed by RMSE. For the MAE and RMSE estimates, equations (7) and (8) were used:

$$MAE = \frac{1}{n} \sum_{i=1}^n |a - b| \quad (10)$$

$$RMSE = \sqrt{\frac{1}{n} \sum_{i=1}^n |a - b|^2} \quad (11)$$

where, n is 'the sample size of the training or testing dataset'; a is 'the predicted value', and b is 'the actual values'. Willmott and Matsuura (2005) used this strategy and established a limit value of 0.5. Values beyond 0.5 suggest poor results of the model. Such two tests were used to determine the efficacy of landslide susceptibility models (Roy and Saha, 2021; Saha et al., 2021).

3.5.3. SCAI (seed cell area index)

Suzen and Doyuran introduced the SCAI in 2004. It computed the percent ratio of LS in different LS susceptibility classes. In the case of very a good model, the SCAI value is the highest in the very high LS susceptibility class (Roy et al., 2019). The SCAI was computed following equation 12

$$SCAI = \frac{Ar}{Atv} \quad (12)$$

where Ar = areal extend of susceptibility class in percentage and Atv = percentage of training and validation datasets.

4. Results and discussion

4.1. Results of multi-collinearity test

The TOL and VIF indicate that there is no multicollinearity difficulty amongst LS conditioning variables (Sameen and Pradhan, 2019; Saha and Saha, 2020c). According to the multi-collinearity test (Table 2), the lowest TOL is 0.318 for rainfall. Besides that, the maximum TOL for soil type is 0.914. The lowest and highest VIF values in this research are

Table 2
Multi-collinearity analysis of landslide conditioning factors.

Landslide conditional factors	Collinearity statistics	
	Tolerance	VIF
Slope	0.873	1.279
Elevation	0.435	2.780
Aspect	0.641	1.094
Curvature	0.748	1.143
Rainfall	0.318	2.869
Drainage density	0.715	1.874
Lineament density	0.787	1.465
Distance from Roads	0.908	1.108
Soil types	0.914	1.082
Soil depth	0.875	1.113
Geology	0.764	1.265
Geomorphology	0.821	1.189
Earthquake zone	0.398	2.184
Land-use/Land-cover (LU/LC)	0.873	1.153
TWI	0.906	1.107
STI	0.745	1.350
SPI	0.692	1.448

0.982 and 2.869, respectively (Table 2). It is proved that the chosen eighteen LS conditioning factors in this study field are ideal for modeling the LS susceptibility.

4.2. Analyzing the Relief-F

It is necessary to select appropriate LCFs for better performance and accurate project susceptibility. Relief-F (RelF) method is acknowledged as a proficient attribute selection technique (KutlugSahin and Colkesen, 2019; Saha et al., 2020). RelF was used to calculate the average merit (AM) of different factors. LS affecting factor with positive higher AM is more important for LS susceptibility modeling. Factors with "0" or negative AM are less important for LS susceptibility modeling. According to AM, all the selected factors have a good capability of inducing the landslide in the study area (Table 3).

4.3. Landslide susceptibility maps (LSMs)

The eight LSMs were created considering 70% of total landslides datasets using MLP, KLR, RF, MARS, MLP-Bagging, KLR-Bagging, RF-Bagging and MARS bagging models in GIS environment (Fig. 5). The areal distributions of different models are given in Table 4. According to the outcomes of the models revealed that the areas of very low LS susceptibility class in MLP, KLR, RF, MARS, MLP-Bagging, KRL-bagging, RF-Bagging and MARS-Bagging models are 76.64 sq.km (20.05%), 84.31 sq.km (22.05%) 99.70 sq.km (26.08%), 103.54 sq.km (27.08%), 99.71 sq.km (26.06%), 84.31sq.km (22.05%), 115.12 sq.km (30.11%), and 99.94 sq.km (26.14%) and moderate LS suspect susceptibility class are 75.74 sq.km (19.81%); 85.91 sq.km (22.47%); 73.91 sq.km (19.33%); 79.93 sq.km (18.83%); 66.95sq.km (17.51%); 91.46 sq.km (23.92%); 73.91 sq.km (19.33%) and 71.99 sq.km (18.83%) respectively. Comparatively high LS susceptibility zone covers 49.90 sq.km (13.05%) in KLR, 46.87 sq.km (12.26%) in MARS-Bagging; 45.57 (11.92%) in RF and 37.77 sq.km (10.14%) in RF-Bagging respectively (Fig. 5). According to the landslide susceptibility models developed, the centre and western sections of the research area are very susceptible to landslides.

4.4. Models performance validation with ROC curve

It is critical to evaluate the legitimacy of the models used for zoning landslide susceptibility since they have no consequences without validation (Arabameri et al., 2020); Saha and Saha, 2020a). The ROC, accuracy, precision, proportion incorrectly classify and SCAI index was used to evaluate the LS susceptible mapping of the Kurseong area.

The outputs of the four ML applied for landslide susceptibility were verified for this study, incorporating data sets collected from the

Table 3
Result of Relief F of landslide conditioning factors.

Selected Factors	Value (Relief F method)
Geomorphology	0.05913
Drainage density	0.03879
Lineament density	0.03505
Road density	0.03319
Geology	0.02949
Slope	0.02705
Altitude	0.02425
LULC	0.01894
Soil depth	0.01863
Soil type	0.01819
Rainfall	0.01711
Aspect	0.01131
TWI	0.00734
Earthquake zone	0.00525
Curvature	0.00222
SPI	0.00199
STI	0.00185

Table 4
Areal distribution of MLP, KLR, RF, MARS, MLP-Bagging, KLR-Bagging, RF-Bagging and MARS-Bagging model for landslide susceptibility classes.

Model	MLP	MLP-Bagging		KLR		KLR-Bagging		RF		RF-Bagging		MARS		MARS-Bagging		
		area in sq.km	% of area													
Very low	76.66	20.05	99.71	26.08	84.31	22.05	99.71	26.08	130.3	34.08	115.12	30.11	103.54	27.08	99.94	26.14
Low	138.22	36.15	130.57	34.15	107.63	28.15	107.63	28.15	103	26.94	105.18	27.51	69.93	18.29	110.31	28.85
Moderate	75.74	19.81	66.95	17.51	85.91	22.47	91.46	23.92	47.33	12.38	73.91	19.33	98.41	25.74	71.99	18.83
High	50.97	13.33	41.45	10.84	54.6	14.28	44.5	11.64	56.13	14.68	49.36	12.91	59.8	15.64	53.18	13.91
Very high	40.76	10.66	43.66	11.42	49.9	13.05	39.04	10.21	45.57	11.92	38.77	10.14	50.66	13.25	46.87	12.26

fieldwork as indicated above. In addition, the AUC was determined to compare the effects of models (Fig. 6). The findings of the ROC curve showed that all the models have great potential for predicting susceptibility to landslides. The AUC-ROC values of the MLP, MLP-Bagging, KLR, KLR-Bagging, RF, RF-Bagging, MARS and MARS-Bagging models are 84.57%, 90.37%, 83.76%, 88.05%, 88.10%, 92.28% and 84.17% & 88.46% for validation dataset and for training dataset AUC-ROC values are 82.95%, 88.75%, 81.98%, 85.53%, 87.89%, 90.85%, and 82.78%, & 86.66% respectively (Table 5). As a consequence, the findings showed that the performance of the MLP, KLR, FR, and MARS models after ensemble with bagging was enhanced by about 2–3% for mapping landslide susceptibility in the Kurseong-Himalayan range. (Fig. 6). The RF-Bagging method achieved the highest accuracy followed by MLP-Bagging, RF, and MLP respectively (Table 5). Contrarily, the RF-Bagging model achieved the lowest proportion of incorrectly classified, MAE and RMSE values followed by the MLP-Bagging, RF, and MLP respectively. In comparison to other models for landslide susceptibility modeling with potential confounders, the RF Bagging technique proved to be the highest.

4.5. Models performance validation by SCAI

Another method applied for the validation of models is SCAI. The SCAI validation method was implemented in LS modeling precision calculation in some current LS research (Khari et al., 2019; Saha and Saha, 2020c). Suzen and Doyuran created this process in 2004. In Table 6 the SCAI values of MLP, MLP-Bagging, RF, and RF-Bagging models are given. From extremely low to very high class, the SCAI value for a suitable model increases. So, SCAI values also proved that the MLP-Bagging model is better than the MLP model and the RF-Bagging better than the RF model. It also proved that all models have very good capability to map the LS susceptibility in this study area.

5. Discussion

5.1. Comparison of models' predictive performance

Several methods were used for determining risks to the environment. Modeling mechanisms and methodology, however, are diverse and have provided specific outcomes and predictive output. GIS-based geographic forecasts using various methods are essential instruments for environmental and spatial-environmental studies which can aid in managing environmental problems (Nasiri et al., 2014; Lombardo et al., 2020). Accessibility to the range of solutions has considerably improved decision-makers willingness to ensure continuity in environmental development (Liu et al., 2008). Saupe et al. (2012) cautioned that the application of modeling methods would produce quite different outcomes and very different outputs in many other domains or with other applications. For this purpose, simulation results evaluations are critical for model efficiency and accuracy assessments (Briand et al., 2000; Stoyanov et al., 2013).

The predictive efficiency of the models for predicting LS susceptibility was compared in this analysis using AUC-ROC, precision, accuracy, proportion incorrectly identified, MAE, RMSE, and SCAI. The eight models (MLP, KLR, RF, MARS, MLP-Bagging, KLR-Bagging, RF-Bagging, and MARS-Bagging) have varying performance. All models showed incredible performance well and the RF-Bagging ensemble model was proven to be the suitable method for prediction. Pham et al. (2016) also used MLP as a basis classifier for the LSM ensemble in the Garhwal Himalayan of India. Azhari et al. (2020) used a bagging-based ANN model in the astrophysical area. Salam and Islam (2020) used RF-bagging to calculate evapotranspiration prediction study in Bangladesh. Specific dependent variables were used to forecast LS susceptibility involving topography (slope, elevation, shape, and curvature), geomorphology (drainage density, SPI, TWI), soil (type and depth), landform, and anthropogenic behavior (LULC, road distance). The main indicator of the LSMs in this analysis is the slope, rainfall, geomorphology, and elevation.

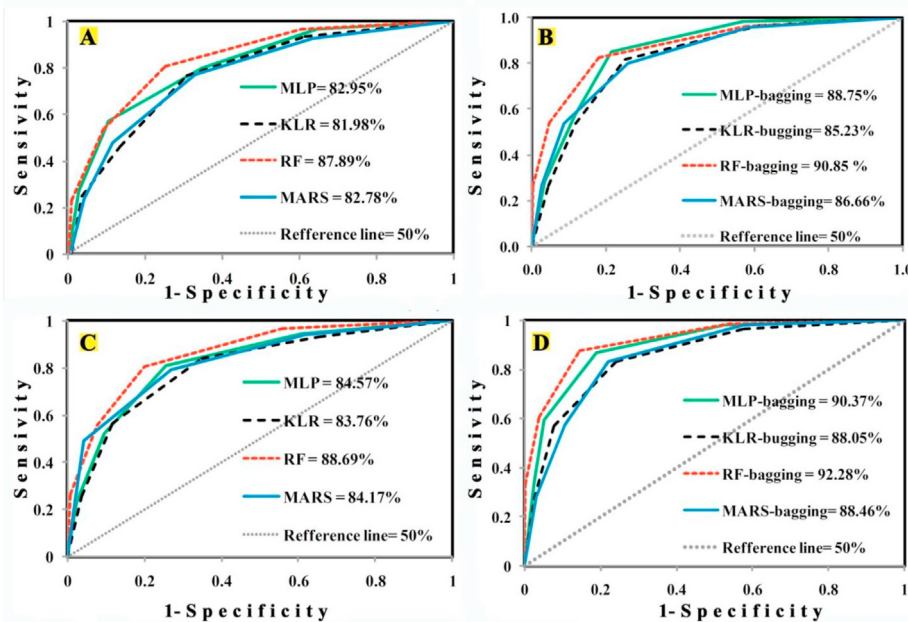


Fig. 6. Validation of landslide models: A. ROC curves of individual machine learning model using training dataset, B. ROC curve of ensemble machine learning technique using training dataset, and C. ROC curves of individual machine learning models using testing dataset, D. ROC curves of ensemble machine learning technique using testing dataset.

Table 5

Values of ROC, Precision, Accuracy, Proportion incorrectly classified, MAE and RMSE methods.

Datasets	Model	Precision	Accuracy	Proportion incorrectly classified	Over all	MAE	RMSE
					AUC (%)		
Training	MLP	0.804	0.815	0.208	82.95	0.423	0.098
	MLP-Bagging	0.819	0.841	0.139	88.75	0.313	0.179
Validate	MLP	0.923	0.833	0.181	84.57	0.244	0.098
	MLP-Bagging	0.857	0.879	0.139	90.37	0.252	0.118
Training	KLR	0.845	0.801	0.198	81.98	0.268	0.151
	KLR-Bagging	0.882	0.824	0.185	85.53	0.246	0.131
Validate	KLR	0.874	0.789	0.202	83.76	0.324	0.148
	KLR-Bagging	0.894	0.823	0.176	88.05	0.269	0.134
Training	RF	0.905	0.895	0.167	87.89	0.486	0.237
	RF-Bagging	0.917	0.917	0.111	90.85	0.302	0.098
Validate	RF	0.923	0.923	0.124	88.07	0.345	0.125
	RF-Bagging	0.948	0.947	0.083	92.28	0.213	0.074
Training	MARS	0.791	0.799	0.201	82.78	0.377	0.165
	MARS-Bagging	0.874	0.824	0.187	86.66	0.268	0.133
Validate	MARS	0.867	0.873	0.137	84.17	0.299	0.136
	MARS bagging	0.913	0.878	0.122	88.46	0.235	0.107

Ensemble meta-classifiers enhanced a single benchmark model's (MLP, KLR, RF, and MARS) prediction capability. Ensemble MLTs efficiently boost base classifier performance (Roy and Saha, 2021; Pham et al., 2016; Saha and Saha, 2020c). This whole study provided outstanding performance by bagging the ensemble with RF, KLR, MLP, and MARS relative to the individual models (Table 5). Bagging ensembles significantly reduced both ambiguity and biases most efficiently relative to other ensembles. The tree-based approach to artificial intelligence can effectively address those bias issues (Silva et al., 2015). More precisely, the study found, despite the complete lack of proper statistical testing for ML models may restrict probabilistic testing of the proposition, that the RF-bagging model is in a position to classify the complex or non-linear relationships between LS and non-LS. Recent studies have proposed that ML algorithms are more appropriate for LS research than statistical approaches (Duro et al., 2012; Saha and Saha, 2020a; Azhar et al., 2020; Saha and Saha, 2020c).

AUC-ROC values > 0.8, in particular, suggest outstanding results as well. The areal distribution of the four benchmark models (MLP, KLR,

RF, & MARS) and four novel hybrid models (MLP-Bagging, KLR-bagging, RF-Bagging, and MARS-Bagging) is not the same (Fig. 6). For this study we find that RF-Bagging (testing AUC = 92.28%; training AUC = 90.85%) output is outstanding while the selected benchmark model KLR (AUC training = 81.98%; testing = 83.76%), MARS (AUC training = 82.78%; testing = 84.17%), and MLP (AUC training = 82.95%; testing = 84.57%) model's consistency is just quite fine. The other methods of validation (precision, accuracy, MAE, and RMSE) and SCAI give a related performance. Across all efficiency measures, the RF-Bagging had the best and KLR alone the lowest precision (Table 6). Previous research (Dunne et al., 2020; Rahmati et al., 2019) deduced that the LS forecasting of ML models would enhance in comparison with traditional methods. After all, results may be different depending on the region where and the variables utilized.

5.2. Contribution of LCFs analyzed by RF

The LCFs' relevance evaluation is critical for environmental resources management (Sameen et al., 2020). Arabameri et al. (2020) suggested

Table 6

Seed cell area index (SCAI) of different landslide susceptibility maps.

Model/Method	Classes	Training Area (TA) in km ²		Validation area (LA) in km ²		Sum (TA% + LA %)	SCAI value
		area	%	area	%		
MLP	Very low	0.029	0.0531	0.005	0.004	0.057	17.54
	low	0.075	0.1373	0.031	0.024	0.162	6.19
	Moderate	0.104	0.1904	0.128	0.1	0.291	3.44
	High	0.219	0.401	0.142	0.111	0.512	1.95
	Very high	0.962	1.7614	0.688	0.54	2.302	0.43
	Very low	0.043	0.0787	0.011	0.009	0.087	11.45
KLR	low	0.094	0.1721	0.031	0.024	0.196	5.09
	Moderate	0.159	0.2911	0.118	0.093	0.384	2.61
	High	0.239	0.4376	0.167	0.131	0.569	1.76
	Very high	0.854	1.5637	0.668	0.524	2.088	0.48
	Very low	0.026	0.0476	0.006	0.004	0.052	19.26
	low	0.076	0.1392	0.032	0.025	0.164	6.09
RF	Moderate	0.119	0.2179	0.119	0.093	0.311	3.22
	High	0.202	0.3699	0.134	0.105	0.475	2.11
	Very high	0.967	1.7697	0.706	0.554	2.323	0.43
	Very low	0.049	0.0897	0.011	0.009	0.098	10.17
	Low	0.106	0.1941	0.051	0.04	0.234	4.27
	Moderate	0.186	0.3406	0.107	0.084	0.425	2.36
MARS	High	0.335	0.6134	0.152	0.119	0.733	1.36
	Very high	0.713	1.3055	0.674	0.529	1.835	0.55
	Very low	0.023	0.0412	0.006	0.005	0.046	21.78
	low	0.077	0.141	0.033	0.026	0.166	6.01
	Moderate	0.134	0.2454	0.109	0.085	0.331	3.03
	High	0.185	0.3387	0.125	0.098	0.437	2.29
MLP-Bagging	Very high	0.971	1.777	0.723	0.567	2.344	0.43
	Very low	0.039	0.0714	0.008	0.006	0.078	12.87
	Low	0.091	0.1657	0.041	0.032	0.198	5.05
	Moderate	0.145	0.2655	0.118	0.092	0.358	2.8
	High	0.277	0.5072	0.147	0.115	0.623	1.61
	Very High	0.838	1.5335	0.681	0.535	2.068	0.48
RF-Bagging	Very low	0.016	0.0293	0.007	0.005	0.035	28.74
	Low	0.079	0.1446	0.034	0.027	0.171	5.84
	Moderate	0.164	0.3003	0.089	0.07	0.37	2.7
	High	0.151	0.2765	0.108	0.085	0.361	2.77
	Very High	0.979	1.7925	0.757	0.594	2.387	0.42
	Very low	0.036	0.0659	0.008	0.006	0.072	13.85
MARS-Bagging	Low	0.085	0.1547	0.031	0.024	0.179	5.58
	Moderate	0.132	0.2408	0.123	0.097	0.337	2.96
	High	0.229	0.4193	0.155	0.121	0.541	1.85
	Very High	0.908	1.6625	0.678	0.532	2.195	0.46

that a quantitative evaluation of the correlations between LCFs and LS enable planner and stakeholders to predict the impacts of LCFs. The conditioning variables which work well in one simulation can therefore be negligible in other simulations. For this research work, the significant contribution of LCFs in numerous previous studies was assessed using an RF model (Rahmati et al., 2019). The findings of the RF model revealed that slope had the largest weight and soil depth had the least weight

(Table 7). Other high weights were produced by geomorphology, elevation, the density of runoff, rainfall, and road density.

6. Conclusions

The natural hazards damage the infrastructural facilities and human lives, however, among these LS is more destructive. Benchmark models (i.e. MLP, KLR, RF, and MARS) and novel hybrid ensembles (i.e. MLP-Bagging, KLR-Bagging, RF-Bagging, and MARS-Bagging) models were applied in this study to evaluate susceptibility to LS in Kurseong region of Darjeeling Himalaya. The LS inventory map was partitioned into training (70%) and testing (30%) samples. In this analysis, we implemented four individual and four ensemble ML approaches (MLP, KLR, RF, MARS, MLP-Bagging, KLR-Bagging, RF-Bagging, and MARS-Bagging). ML methods were established based on prior LS cases (303) and the models were trained. These techniques achieved quite better precision, although the ensemble ML algorithm MLP-Bagging, KLR-Bagging, RF-Bagging, and MARS-bagging provided much more accurate results. The fallow terrain, the forest plantations, roadside places, highly sloppy area and natural denudation mountain regions, are more susceptible to landslides in comparison with the rest of the Kurseong-Himalayan region. Descriptive data of LS susceptibility maps can also identify places with the highest vulnerability, and sites needing more intense attention and study. The susceptibility maps will significantly benefit the local people and government in managing and reducing the losses caused by the landslides.

Table 7

Values of mean decrease Gini using RF model.

Selected Factors	Mean decrease Gini
Slope	175.309
Geomorphology	133.361
Altitude	131.094
Drainage density	114.203
Rainfall	112.325
Road density	103.968
Lineament density	95.041
NDVI	89.255
Aspect	84.351
LULC	77.240
TWI	72.263
Curvature	62.055
SPI	59.345
STI	46.434
Soil type	42.622
Geology	42.385
Earthquake zone	26.649
Soil depth	26.330

Funding

No funding was received for this work.

Declaration of competing interests

The authors declare that they have no known competing financial interests or personal relationships that could have appeared to influence the work reported in this paper.

CRDiT authorship contribution statement

Anik Saha: Methodology, Formal analysis, Investigation, Writing – original draft, Software. **Sunil Saha:** Methodology, Formal analysis, Investigation, Writing – original draft, Writing – review & editing.

Acknowledgments

The authors would like to thank the inhabitants of Basin because they have helped a lot during our field visit. At last, the authors would like to acknowledge all of the agencies and individuals especially, the Survey of India (SOI), Geological Survey of India (GSI), and USGS for obtaining the maps and data required for the study.

References

- Afanador, E.G., Kjelland, M.E., Wu, X.B., Wilkins, N., Grant, W.E., 2016. Ownership property size, landscape structure, and spatial relationships in the Edwards Plateau of Texas (USA): landscape scale habitat management implications. *Environ. Syst. Decis.* 36 (3), 310–328.
- Amato, G., Eisank, C., Castro-Camilo, D., Lombardo, L., 2019. Accounting for covariate distributions in slope-unit-based landslide susceptibility models. A case study in the alpine environment. *Eng. Geol.* 260, 105237.
- Arabameri, A., Saha, S., Roy, J., Chen, W., Blaschke, T., Tien Bui, D., 2020. Landslide susceptibility evaluation and management using different machine learning methods in the gallicash river watershed, Iran. *Rem. Sens.* 12 (3), 475. <https://doi.org/10.3390/rs12030475>.
- Aristizábal, E., Sánchez, O., 2020. Spatial and temporal patterns and the socioeconomic impacts of landslides in the tropical and mountainous Colombian Andes. *Disasters* 44 (3), 596–618.
- Azhari, M., Abarda, A., Alaoui, A., Ettaki, B., Zerouaoui, J., 2020. Detection of pulsar candidates using bagging method. *Procedia Comput. Sci.* 170, 1096–1101.
- Breiman, L., 1996. Bagging predictors. *Mach. Learn.* 24 (2), 123–140.
- Briand, L.C., Langley, T., Wieczorek, I., 2000, June. A replicated assessment and comparison of common software cost modeling techniques. In: Proceedings of the 22nd International Conference on Software Engineering, pp. 377–386.
- Bui, D.T., Tuan, T.A., Klempe, H., Pradhan, B., Revhaug, I., 2016. Spatial prediction models for shallow landslide hazards: a comparative assessment of the efficacy of support vector machines, artificial neural networks, kernel logistic regression, and logistic model tree. *Landslides* 13 (2), 361–378.
- Cama, M., CristiNiciu, I., Conoscenti, C., Quénéhervé, G., Maerker, M., 2016, April. The role of multicollinearity in landslide susceptibility assessment by means of Binary Logistic Regression: comparison between VIF and AIC stepwise selection. In: EGU General Assembly Conference Abstracts, vol. 18.
- Chan, J.C.W., Paelinckx, D., 2008. Evaluation of Random Forest and Adaboost tree-based ensemble classification and spectral band selection for ectope mapping using airborne hyperspectral imagery. *Rem. Sens. Environ.* 112 (6), 2999–3011.
- Chauhan, J.S., Gautam, A.S., Negi, R.S., 2018. Natural and anthropogenic impacts on forest structure: a case study of Uttarakhand State. *Open Environ. Res.* J. 11 (1).
- Chawla, A., Chawla, S., Pasupuleti, S., Rao, A.C.S., Sarkar, K., Dwivedi, R., 2018. Landslide susceptibility mapping in Darjeeling Himalayas, India. *Adv. Civ. Eng.* 2018.
- Chen, W., Ding, X., Zhao, R., Shi, S., 2016. Application of frequency ratio and weights of evidence models in landslide susceptibility mapping for the Shangzhou District of Shangqiu City, China. *Environ. Earth Sci.* 75 (1), 64.
- Chen, X., Chen, W., 2021. GIS-based landslide susceptibility assessment using optimized hybrid machine learning methods. *Catena* 196, 104833.
- Cutler, D.R., Edwards Jr., T.C., Beard, K.H., Cutler, A., Hess, K.T., Gibson, J., Lawler, J.J., 2007. Random forests for classification in ecology. *Ecology* 88 (11), 2783–2792.
- Dang, V.H., Hoang, N.D., Nguyen, L.M.D., Bui, D.T., Samui, P., 2020. A novel GIS-based random forest machine algorithm for the spatial prediction of shallow landslide susceptibility. *Forests* 11 (1), 118. <https://doi.org/10.3390/f11010118>.
- Dunne, K.S., Holden, N.M., O'Rourke, S.M., Fenlon, A., Daly, K., 2020. Prediction of phosphorus sorption indices and isotherm parameters in agricultural soils using mid-infrared spectroscopy. *Geoderma* 358, 113981.
- Duro, D.C., Franklin, S.E., Dubé, M.G., 2012. A comparison of pixel-based and object-based image analysis with selected machine learning algorithms for the classification of agricultural landscapes using SPOT-5 HRG imagery. *Rem. Sens. Environ.* 118, 259–272.
- Gardner, M.W., Dorling, S.R., 1998. Artificial neural networks (the multilayer perceptron)—a review of applications in the atmospheric sciences. *Atmos. Environ.* 32 (14–15), 2627–2636.
- Gayen, A., Pourghasemi, H.R., Saha, S., Keesstra, S., Bai, S., 2019. Gully erosion susceptibility assessment and management of hazard-prone areas in India using different machine learning algorithms. *Sci. Total Environ.* 668, 124–138. <https://doi.org/10.1016/j.scitotenv.2019.02.436>.
- Genuer, R., Poggi, J.M., Tuleau-Malot, C., 2010. Variable selection using random forests. *Pattern Recogn. Lett.* 31 (14), 2225–2236.
- Groesser, S., Schwaninger, M., 2012. Contributions to model validation: hierarchy, process, and cessation. *Syst. Dynam. Rev.* 28 (2), 157–181.
- Haykin, S., 2009. *Neural networks and learning machines*, 3/E. Pearson Education, India.
- Hirota, K., Konagai, K., Sassa, K., Dang, K., Yoshinaga, Y., Wakita, E.K., 2019. Landslides triggered by the west Japan heavy rain of July 2018, and geological and geomorphological features of soaked mountain slopes. *Landslides* 16 (1), 189–194.
- Juliev, M., Mergili, M., Mondal, I., Nurtaev, B., Pulatov, A., Hübl, J., 2019. Comparative analysis of statistical methods for landslide susceptibility mapping in the Bostanlik District, Uzbekistan. *Sci. Total Environ.* 653, 801–814.
- Khamkar, D.J., Mhaske, S.Y., 2019. Identification of landslide susceptible settlements using geographical information system of Yelwandi river basin, Maharashtra (India). *Nat. Hazards* 1–25.
- Khari, M., Garg, A.K., Gandomi, A.H., Gupta, R., Patan, R., Balusamy, B., 2019. Securing data in Internet of Things (IoT) using cryptography and steganography techniques. *IEEE Trans. Syst. Man Cybern. Syst.* 50 (1), 73–80.
- Khosravi, K., Pham, B.T., Chapi, K., Shirzadi, A., Shahabi, H., Revhaug, I., Bui, D.T., 2018. A comparative assessment of decision trees algorithms for flash flood susceptibility modeling at Haraz watershed, northern Iran. *Sci. Total Environ.* 627, 744–755.
- Koley, B., Nath, A., Saraswati, S., Bandyopadhyay, K., Ray, B.C., 2019. Assessment of rainfall thresholds for rain-induced landslide activity in North Sikkim road Corridor in Sikkim Himalaya, India. *J. Geog. Environ. Earth Sci. Int.* 1–14.
- Kononenko, I., 1994, April. Estimating attributes: analysis and extensions of RELIEF. In: European Conference on Machine Learning. Springer, Berlin, Heidelberg, pp. 171–182.
- Kornejady, A., Pourghasemi, H.R., Afzali, S.F., 2019. Presentation of RFFR new ensemble model for landslide susceptibility assessment in Iran. In: *Landslides: Theory, Practice and Modelling*. Springer, Cham, pp. 123–143.
- KutlugSahin, E., Colkesen, I., 2019. Performance analysis of advanced decision tree-based ensemble learning algorithms for landslide susceptibility mapping. *Geocarto Int.* 1–23.
- Liao, Z., Liao, Z., 2020. Slope stability evaluation using backpropagation neural networks and multivariate adaptive regression splines. *Open Geosci.* 12 (1), 1263–1273.
- Lin, C.H., Jan, J.C., Pu, H.C., Tu, Y., Chen, C.C., Wu, Y.M., 2015. Landslide seismic magnitude. *Earth Planet Sci. Lett.* 429, 122–127.
- Liu, Y., Gupta, H., Springer, E., Wagener, T., 2008. Linking science with environmental decision making: Experiences from an integrated modeling approach to supporting sustainable water resources management. *Environ. Model. Software* 23 (7), 846–858.
- Lombardo, L., Opitz, T., Ardizzone, F., Guzzetti, F., Huser, R., 2020. Space-time landslide predictive modelling. *Earth Sci. Rev.* 209, 103318.
- Mahdafi, F., Boumezbeur, A., Hadji, R., Kanungo, D.P., Zahri, F., 2018. GIS-based landslide susceptibility assessment using statistical models: a case study from Souk Ahras province, NE Algeria. *Arabian J. Geosci.* 11 (17), 476.
- Marjanović, M., 2013. Comparing the performance of different landslide susceptibility models in ROC space. In: *Landslide Science and Practice*. Springer, Berlin, Heidelberg, pp. 579–584.
- Meng, Q., Miao, F., Zhen, J., Wang, X., Wang, A., Peng, Y., Fan, Q., 2016. GIS-based landslide susceptibility mapping with logistic regression, analytical hierarchy process, and combined fuzzy and support vector machine methods: a case study from Wolong Giant Panda Natural Reserve, China. *Bull. Eng. Geol. Environ.* 75 (3), 923–944.
- Mercer, J., 1909. XVI. functions of positive and negative type, and their connection with the theory of integral equations. *Philos. Trans. R. Soc. Lond. - Ser. A Contain. Pap. a Math. or Phys. Character* 209 (441–458), 415–446.
- Nasiri, F., Ikediashi, D.I., Ogunkana, S.O., Ujene, A.O., 2014. An investigation on policy direction and drivers for sustainable facilities management practice in Nigeria. *J. Facil. Manag.*
- Nguyen, K.A., Chen, W., Lin, B.S., Seeboonruang, U., 2021. Comparison of ensemble machine learning methods for soil erosion pin measurements. *ISPRS Int. J. Geo-Inf.* 10 (1), 42.
- Nsengiyumva, J.B., Luo, G., Amanambu, A.C., Mind'je, R., Habiyaremye, G., Karamage Ochege, F.U., Mupenzi, C., 2019. Comparing probabilistic and statistical methods in landslide susceptibility modeling in Rwanda/Centre-Eastern Africa. *Sci. Total Environ.* 659, 1457–1472.
- Ozioko, O.H., Igwe, O., 2020. GIS-based landslide susceptibility mapping using heuristic and bivariate statistical methods for Iva Valley and environs Southeast Nigeria. *Environ. Monit. Assess.* 192 (2), 1–19. <https://doi.org/10.1007/s10661-019-7951-9>.
- Pecoraro, G., Calvello, M., Cepeda, J.M., 2019. Using local monitoring data for regional forecasting of weather-induced landslides in Norway. In: 17th European Conference on Soil Mechanics and Geotechnical Engineering, pp. 1–6. Sep.
- Pham, B.T., Pradhan, B., Bui, D.T., Prakash, I., Dholakia, M.B., 2016. A comparative study of different machine learning methods for landslide susceptibility assessment: a case study of Uttarakhand area (India). *Environ. Model. Software* 84, 240–250.
- Pisano, L., Zumpano, V., Malek, Ž., Rosskopf, C.M., Parise, M., 2017. Variations in the susceptibility to landslides, as a consequence of land cover changes: a look to the past, and another towards the future. *Sci. Total Environ.* 601, 1147–1159.
- Rahmati, O., Kornejady, A., Samadi, M., Deo, R.C., Conoscenti, C., Lombard, L., et al., 2019. PMT: new analytical framework for automated evaluation of geo-environmental modelling approaches. *Sci. Total Environ.* 664, 296–311.

- Reichenbach, P., Rossi, M., Malamud, B.D., Mihir, M., Guzzetti, F., 2018. A review of statistically-based landslide susceptibility models. *Earth Sci. Rev.* 180, 60–91.
- Rodriguez-Galiano, V.F., Ghimire, B., Rogan, J., Chica-Olmo, M., Rigol-Sánchez, J.P., 2012. An assessment of the effectiveness of a random forest classifier for land-cover classification. *ISPRS J. Photogrammetry Remote Sens.* 67, 93–104.
- Roy, J., Saha, S., 2021. Integration of artificial intelligence with meta classifiers for the gully erosion susceptibility assessment in Hinglo river basin, Eastern India. *Adv. Space Res.* 67 (1), 316–333.
- Roy, J., Saha, S., Arabameri, A., Blaschke, T., Bui, D.T., 2019. A novel ensemble approach for landslide susceptibility mapping (LSM) in Darjeeling and Kalimpong Districts, West Bengal, India. *Rem. Sens.* 11 (23), 2866.
- Saha, A., Saha, S., 2020c. Comparing the efficiency of weight of evidence, support vector machine and their ensemble approaches in landslide susceptibility modelling: a study on Kurseong region of Darjeeling Himalaya, India. *Remote Sens. Appl. Soc. Environ.*, 100323 <https://doi.org/10.1016/j.rsase.2020.100323>.
- Saha, A., Saha, S., 2020a. Application of statistical probabilistic methods in landslide susceptibility assessment in Kurseong and its surrounding area of Darjeeling Himalayan, India: RS-GIS approach. *Environ. Dev. Sustain.* <https://doi.org/10.1007/s10668-020-00783-1>.
- Saha, S., Arabameri, A., Saha, A., Blaschke, T., Ngo, P.T.T., Nhu, V.H., Band, S.S., 2021. Prediction of landslide susceptibility in Rudraprayag, India using novel ensemble of conditional probability and boosted regression tree-based on cross-validation method. *Sci. Total Environ.*, 142928 <https://doi.org/10.1016/j.scitotenv.2020.142928>.
- Saha, S., Saha, A., Hembram, T.K., Pradhan, B., Alamri, A.M., 2020. Evaluating the performance of individual and novel ensemble of machine learning and statistical models for landslide susceptibility assessment at Rudraprayag District of Garhwal Himalaya. *Appl. Sci.* 10 (11), 3772. <https://doi.org/10.3390/app1013772>.
- Saha, S., Saha, A., Hembram, T.K., Mandal, K., Sarkar, R., Bhardwaj, D., 2022. Prediction of spatial landslide susceptibility applying the novel ensembles of CNN, GLM and random forest in the Indian Himalayan region. *Stoch. Environ. Res. Risk Assess.* 1–20.
- Salam, R., Islam, A.R.M.T., 2020. Potential of RT, Bagging and RS ensemble learning algorithms for reference evapotranspiration prediction using climatic data-limited humid region in Bangladesh. *J. Hydrol.* 590, 125241.
- Sameen, M.I., Pradhan, B., 2019. Landslide detection using Residual networks and the fusion of spectral and topographic information. *IEEE Access* 7, 114363–114373.
- Sameen, M.I., Pradhan, B., Lee, S., 2020. Application of convolutional neural networks featuring Bayesian optimization for landslide susceptibility assessment. *Catena* 186, 104249. <https://doi.org/10.1016/j.catena.2019.104249>.
- Saupe, E.E., Barve, V., Myers, C.E., Soberón, J., Barve, N., Hensz, C.M., et al., 2012. Variation in niche and distribution model performance: the need for a priori assessment of key causal factors. *Ecol. Model.* 237, 11–22.
- Shahbazi, B., Chelgani, S.C., Matin, S.S., 2017. Prediction of froth flotation responses based on various conditioning parameters by Random Forest method. *Colloids Surf. A Physicochem. Eng. Asp.* 529, 936–941.
- Silva, L.T., Sampao, E.P.F.F.M., Corte-Real, J.A.M., Rodriguez, D.A., Medeiros, F.C., Moraes, B.E., França, D.G.M., 2015. Susceptibility and vulnerability to landslides—case study: basin of river Bengalias—City of Nova Friburgo—Brazil. In: *Engineering Geology for Society and Territory*, vol. 1. Springer, Cham, pp. 539–546.
- Srivastava, S., Priyadarshini, J., Gopal, S., Gupta, S., Dayal, H.S., 2019. Optical character recognition on bank Cheques using 2D Convolution neural network. In: *Applications of Artificial Intelligence Techniques in Engineering*. Springer, Singapore, pp. 589–596.
- Stoyanov, T., Magnusson, M., Lilienthal, A.J., 2013. Comparative evaluation of the consistency of three-dimensional spatial representations used in autonomous robot navigation. *J. Field Robot.* 30 (2), 216–236.
- Sugiyama, M., Simm, J., 2010, August. A computationally-efficient alternative to kernel logistic regression. In: *2010 IEEE International Workshop on Machine Learning for Signal Processing*. IEEE, pp. 124–129.
- Talukdar, S., Ghose, B., Salam, R., Mahato, S., Pham, Q.B., Linh, N.T.T., et al., 2020. Flood susceptibility modeling in Teesta River basin, Bangladesh using novel ensembles of bagging algorithms. *Stoch. Environ. Res. Risk Assess.* 34 (12), 2277–2300.
- Tien Bui, D., Khosravi, K., Shahabi, H., Daggupati, P., Adamowski, J.F., Melesse, A.M., et al., 2019. Flood spatial modeling in northern Iran using remote sensing and GIS: a comparison between evidential belief functions and its ensemble with a multivariate logistic regression model. *Rem. Sens.* 11 (13), 1589. <https://doi.org/10.3390/rs11131589>.
- Wang, B., Li, J., Jin, X., Xiao, H., 2019. Mapping tea plantations from multi-seasonal Landsat-8 OLI imageries using a random forest classifier. *J. Indian Soc. Rem. Sens.* 47 (8), 1315–1329.
- Wang, T., Ma, H., Liu, J., Luo, Q., Wang, Q., Zhan, Y., 2021. Assessing frost heave susceptibility of gravelly soils based on multivariate adaptive regression splines model. *Cold Reg. Sci. Technol.* 181, 103182.
- Wang, Z., Zhang, Y., Chen, Z., Yang, H., Sun, Y., Kang, J., Yang, Y., Liang, X., 2016. Application of ReliefF algorithm to selecting feature sets for classification of high resolution remote sensing image. In: *2016 IEEE International Geoscience and Remote Sensing Symposium (IGARSS)*. IEEE, pp. 755–758.
- Willmott, C.J., Matsuura, K., 2005. Advantages of the mean absolute error (MAE) over the root mean square error (RMSE) in assessing average model performance. *Clim. Res.* 30 (1), 79–82.
- Zhou, C., Yin, K., Cao, Y., Ahmed, B., Li, Y., Catani, F., Pourghasemi, H.R., 2018. Landslide susceptibility modeling applying machine learning methods: a case study from Longji in the Three Gorges Reservoir area, China. *Comput. Geosci.* 112, 23–37. <https://doi.org/10.1016/j.cageo.2017.11.019>.